# [$^{11}$C]PBR28 radiotracer kinetics are not driven by alterations in cerebral blood flow

Christin Y Sander[1,2] (ID), Stefano Bovo[1,3] (ID),
Angel Torrado-Carvajal[1,4] (ID), Daniel Albrecht[1],
Hongping Deng[1] (ID), Vitaly Napadow[1,2], Julie C Price[1,2],
Jacob M Hooker[1,2] and Marco L Loggia[1,2]

## Abstract
The positron emission tomography (PET) radiotracer [$^{11}$C]PBR28 has been increasingly used to image the translocator protein (TSPO) as a marker of neuroinflammation in a variety of brain disorders. Interrelatedly, similar clinical populations can also exhibit altered brain perfusion, as has been shown using arterial spin labelling in magnetic resonance imaging (MRI) studies. Hence, an unsolved debate has revolved around whether changes in perfusion could alter delivery, uptake, or washout of the radiotracer [$^{11}$C]PBR28, and thereby influence outcome measures that affect interpretation of TSPO upregulation. In this simultaneous PET/MRI study, we demonstrate that [$^{11}$C]PBR28 signal elevations in chronic low back pain patients are not accompanied, in the same regions, by increases in cerebral blood flow (CBF) compared to healthy controls, and that areas of marginal hypoperfusion are not accompanied by decreases in [$^{11}$C]PBR28 signal. In non-human primates, we show that hypercapnia-induced increases in CBF during radiotracer delivery or washout do not alter [$^{11}$C]PBR28 outcome measures. The combined results from two methodologically distinct experiments provide support from human data and direct experimental evidence from non-human primates that changes in CBF do not influence outcome measures reported by [$^{11}$C]PBR28 PET imaging studies and corresponding interpretations of the biological meaning of TSPO upregulation.

## Introduction

The radiotracer [$^{11}$C]PBR28 has been used in brain positron emission tomography (PET) imaging studies to image the 18-kDA translocator protein (TSPO).[1,2] TSPO is upregulated in activated microglia, reactive astrocytes and macrophages, and is therefore a putative biomarker of neuroinflammation.[3–5] Using [$^{11}$C] PBR28, studies by our group and others have reported differences in central nervous system levels of TSPO in many conditions relative to matched control groups.[6] While elevations in TSPO levels are more commonly described in patient groups with neurodegenerative[5,7–9] and chronic pain disorders,[3,4,10–12] decreases and/or inconsistent results have been reported in psychiatric

[1]Department of Radiology, Athinoula A. Martinos Center, Massachusetts General Hospital, Charlestown, MA, USA
[2]Harvard Medical School, Boston, MA, USA
[3]Department of Information Engineering, University of Padova, Padova, Italy
[4]Medical Image Analysis and Biometry Laboratory, Universidad Rey Juan Carlos, Madrid, Spain

**Corresponding authors:**
Christin Y Sander, Athinoula A. Martinos Center for Biomedical Imaging, Massachusetts General Hospital, 149 13th Street, Suite 2301, Charlestown, MA 02129, USA.
Email: csander@mgh.harvard.edu

Marco L Loggia, Athinoula A. Martinos Center for Biomedical Imaging, Massachusetts General Hospital, 149 13th Street, Suite 2301, Charlestown, MA 02129, USA.
Email: marco.loggia@mgh.harvard.edu

populations, particularly in substance abuse,[13–15] and psychosis.[16–19]

Importantly, patient populations can demonstrate altered physiology, such as changes in perfusion or diffusion, which could potentially affect radiotracer delivery. For instance, we have previously reported [^{11}C] PBR28 brain signal elevations in chronic low back pain (cLBP),[3] fibromyalgia[10] and migraine,[12] which are conditions that can also be accompanied by increases in regional cerebral blood flow (CBF).[20,21] As such, understanding whether altered CBF can affect [^{11}C]PBR28 radiotracer delivery or target binding and adversely affect study outcomes when comparing disease groups is of central importance for the interpretation of studies employing this radioligand.

Evaluating the impact of physiological alterations (e.g. blood flow) on TSPO signal is of interest also for the assessment of simplified semiquantitative measurements, such as standardized uptake value (SUV) or SUV ratio (SUVR), as possible alternatives to quantitative outcomes like the volume of distribution ($V_T$).[22,23] These simplified measures and ratio metrics have their limitations, including the possible loss of biologically relevant signal (e.g., if the pseudoreference region is itself affected by alterations in TSPO levels), and the generally low agreement with absolute measurements (SUVR correlates well with DVR,[24,25] but is usually not associated with $V_T$); we refer to existing literature[26–31] for a more in depth discussion. On the other hand, provided that certain conditions are met and with the interpretative caveats in the abovementioned literature, these measures can have some practical advantages: for instance, they do not require invasive arterial sampling and, in some cases, were found to have greater sensitivity to detect patient-control differences due to lower variability.[32] Due to the potential dependency of SUV on blood flow through radiotracer delivery and/or clearance, possibly under non-equilibrium transient conditions, such outcome parameters could theoretically be influenced by alterations in CBF. Ratios can also be impacted if delivery differs between target and reference tissues. It is thus important to formally evaluate whether blood flow alterations may affect any of these measures, as part of the efforts to assess the appropriateness of their use.

Discussions about the effect of CBF changes on radiotracer binding have repeatedly resurfaced.[33–36] In a previous study, we showed experimental evidence that CBF does not affect radiotracer delivery of neuroreceptor radiotracers using simultaneous PET and magnetic resonance imaging (MRI):[37] By using two dopamine $D_2/D_3$ receptor PET radiotracers ([^{11}C] racloride and [^{18}F]fallypride) together with pseudo-continuous arterial spin labeling (pCASL) during a

hypercapnia challenge, we were able to show that neither the shape of time activity curves nor other outcome parameters like binding potentials were altered even by very large changes in CBF. While these results, together with simulations, indicate that CBF is unlikely to affect radiotracer delivery, it remains to be evaluated experimentally whether [^{11}C]PBR28 signal is affected by blood flow.

The goal of this study was to evaluate whether clinical outcome measures of the radiotracer [^{11}C]PBR28 would be influenced by changes in CBF affecting delivery of the radiotracer. Specifically, we aimed to (i) evaluate whether elevations in [^{11}C]PBR28 signal observed in cLBP patients might be accompanied by concomitant increases in CBF in the same regions. We focus in particular on SUVR with a pseudoreference region as this metric has been previously used in this population. Furthermore, we (ii) test whether large, experimentally-induced transient changes in CBF affect [^{11}C]PBR28 measurements in non-human primates (NHPs), specifically during radiotracer delivery. Evaluating potential CBF contributions to [^{11}C]PBR28 signal will achieve a better understanding of the biological meaning of elevated TSPO levels observed in chronic pain and other conditions.

## Methods

### Human study

15 cLBP patients, with or without radiculopathy (mean & standard deviation age $39 \pm 13$ y/o; 7 female), and 19 pain-free healthy controls (mean age $46 \pm 14$ y/o; 11 female) took part in this study. PET imaging data from these subjects were reported in previous publications.[3,11] All participants were screened for the Ala147Thr polymorphism in the TSPO gene as varying genotypes are known to predict binding affinity for the [^{11}C]PBR28 radiotracer: the Ala/Ala, Ala/Thr and Thr/ Thr genotypes are associated with high, mixed and low affinity to TSPO, respectively.[38] Due to this property, only individuals with high or mixed affinity were included in this study. In the cLBP patients, 3 patients were mixed affinity binders, whereas in the healthy controls, 7 subjects were mixed affinity binders, with the remaining being high affinity binders. This study was conducted at the Athinoula A. Martinos Center for Biomedical Imaging at Massachusetts General Hospital. The protocol and all procedures were approved by the local Institutional Review Board (IRB) and the Radioactive Drug Research Committee (RDRC), and written informed consent was obtained from all participants. The conduct of the study was guided by the Ethical Principles and Guidelines for

the Protection of Human Subjects of Research, generally known as the Belmont Report.

*PET/MR image acquisition.* All subjects underwent brain imaging with a brain-dedicated integrated PET/MRI scanner, consisting of a dedicated avalanche photodiode-based BrainPET insert operating in the bore of a 3 T Tim Trio MR scanner (Siemens AG, Healthcare Sector, Erlangen, Germany), equipped with an 8-channel head coil. PET data were acquired for 90 minutes after [11C]PBR28 radiotracer injection. Pseudo-continuous ASL (pCASL) data consisted of 45 pairs of tagged-control images (pCASL label duration = 1.5 s, post-labeling delay = 1 s, TI = 2.5 s, TR = 5 s) and an $M_0$ calibration image (TR = 8 s). The PET data from a subset of these participants, but not the ASL data, have been included in previous reports.[3,11] For the purpose of anatomical localization, spatial normalization, as well as generation of attenuation correction maps,[39] a multi-echo MPRAGE image was acquired (TR = 2530 ms, TE1/TE2/TE3/TE4 = 1.64/3.5/5.36/7.22 ms, flip angle = 7°, voxel size = 1 mm isotropic).

*PET and pCASL image processing.* SUVRs from 60-90 min post-injection PET data were computed as previously described, with whole-brain[3] and occipital cortex[24] used as a pseudoreference region. CBF maps were calculated from motion-corrected pCASL data using the BASIL FSL toolbox (BAT = 1.3 s, $T_{1,tissue}$ = 1.3 s, $T_{1,blood}$ = 1.65 s, alpha = 0.85), based on the Buxton model.[40,41] For each subject, calibration was performed using a single $M_0$ value, using *asl_calib* in BASIL. All images were registered to the MNI152 standard space using FLIRT and FNIRT in FSL[42] and smoothed with a FWHM of 8 mm. Intensity-normalized CBF maps were created by dividing each voxel by the mean of the whole-brain signal prior to smoothing in order to account for global signal differences across subjects.[43–45] CBF data in both absolute and normalized units were used in order to explore the relationship between localized blood flow changes and PET signal. For region of interest (ROI) analyses, mean absolute and normalized CBF and [11C]PBR28 data were extracted from the left and right thalamic region obtained with FIRST in FSL.[46]

*Statistical data analysis.* A voxelwise comparison of pCASL maps in cLBP patients vs. healthy controls was computed with Feat in FSL.[47] This analysis was cluster-corrected using a cluster-forming threshold of $z = 3.1$ and a cluster size threshold of $p = 0.05$. In addition, in order to be sensitive to any changes in perfusion and thus reduce the likelihood of false negatives, we performed a follow-up exploratory analysis using a more liberal cluster-forming threshold of $z = 2.3$ and a cluster size threshold of $p = 0.05$. Three relevant ROIs were investigated in subsequent analyses: the left and right thalamus (anatomically defined using the corresponding labels from the probabilistic Harvard-Oxford Subcortical Atlas [Harvard Center for Morphometric Analysis], thresholded at the arbitrary value of 30), and a "hypoperfusion cluster" (i.e., a cluster associated with lower CBF in patients, as identified in the voxelwise group analyses; see results).

In order to test whether observed changes in [11C] PBR28 signal in cLBP patients might be linked to differences in perfusion, we performed several analyses. All statistical tests included TSPO genotype as a covariate. Normality of the data was assessed using the Shapiro-Wilk test as well as by inspection of the quantile-quantile (QQ) plot. Age differences between groups were not significant and hence were not included as a covariate. First, we evaluated whether regions previously shown to demonstrate [11C]PBR28 signal elevations in patients (left and right thalamic labels)[3] were also accompanied by changes in CBF, using an unpaired t-test and genotype as a covariate. Note that because the participants included in this study only partially overlapped with those included in prior publications, the presence of significantly elevated thalamic [11C]PBR28 signal was confirmed in the specific sample included in this study, by performing an ANOVA, correcting for TSPO genotype.

Second, we tested for group differences in [11C] PBR28 signal in regions demonstrating group differences in CBF (hypoperfusion cluster), using an ANOVA and correcting for TSPO genotype. In the group analyses, we evaluated both whole-brain normalized as well as absolute CBF in the group analyses, and [11C]PBR28 signal was quantified as SUVR relative to either whole-brain or occipital cortex (two previously used pseudoreference regions for [11C] PBR28).[24]

Finally, using multiple regression with TSPO genotype as a covariate, we tested for the presence of significant associations between [11C]PBR28 signal and normalized CBF within selected regions (i.e., the only signals demonstrating any group differences).

## Non-human primate study

Two female baboons (*papio anubis,* 9 y/o, 16.5 ± 1.5 kg average weight at each scan) underwent simultaneous PET/MR imaging with three imaging sessions each. The baboons were anesthetized (induction with 0.5 mg/kg xylazine and 10 mg/kg ketamine, then maintenance throughout the scan with 1.5% isoflurane). Physiological monitoring was continuous throughout the study and included blood pressure, heart rate,

end-tidal $CO_2$ and breathing rate. The baboons were ventilated during the hypercapnia scan sessions (see below). All procedures were approved by and complied with the regulations of the Institutional Animal Care and Use Committees (IACUC) at Massachusetts General Hospital. All animal experiments were conducted according to the Guide for the Care and Use of Laboratory Animals and are reported in compliance with the ARRIVE guidelines.

*PET/MR image acquisition & reconstruction.* Images were acquired on a whole-body human PET/MR scanner at 3 T (mMR, Siemens AG, Healthcare Sector, Erlangen, Germany). The radiotracer [11C]PBR28 was injected as a bolus by hand and dynamic image acquisition of PET emission data in list mode lasted for 90 minutes, starting with the injection of the radiotracer. Injected activities were similar for each scan, with an average of $5.98 \pm 0.09$ mCi. Arterial blood sampling was done in all studies but was only partially acquired in one hypercapnia scan in one animal due to a temporarily dislocated arterial line and in one baseline scan in the other animal due to failed metabolite correction (see kinetic modeling section for how this was addressed). Images were reconstructed with an ordinary Poisson expectation maximization algorithm with 3 iterations and 21 subsets. Corrections for scatter and attenuation were applied during reconstruction. The dynamic PET data volumes comprised of $4 \times 4 \times 2$ mm voxels in a $172 \times 172 \times 172$ matrix, and time bins of $10 \times 30$ s, followed by 1 min frames.

A custom-built PET compatible 8-channel NHP receive array was used for MR image acquisitions.[48] Pseudo-continuous ASL parameters were adopted for NHPs[49] and were acquired throughout the entire study duration (FOV $= 128 \times 128 \times 80$ mm, resolution $= 2 \times 2 \times 4$ mm, TE $= 15$ ms, TR $= 4$ s, flip angle $= 90°$, number of RF pulse blocks $= 114$, with labeling duration $= 2.2$ s, post-labeling delay $= 800$ ms, bandwidth $= 1906$ Hz/pixel). A two-fold acceleration with GRAPPA was used in the anterior-posterior direction. Cerebral blood flow (CBF) was measured during the entire [11C]PBR28 acquisition.

*Hypercapnia study design.* Each animal received a brain [11C]PBR28 PET/MRI scan under normocapnic and hypercapnic conditions ("baseline" and "hypercapnia scans"), with one set of scans completed on the same day and all remaining ones on separate days and spaced out by at least one month. In the baseline scans, the animals were continually ventilated on normal air. In the hypercapnia scans, the animals were administered a 7% $CO_2$ gas challenge starting 3 min before time of injection (TOI) and continuing until 12 min post-TOI, then additionally at 30–45 min

and 65–80 min after TOI. The hypercapnia blocks were interleaved with normocapnia blocks, i.e. with the NHP ventilated on normal air, for safety reasons and so that maximum blood flow increase could be achieved without the animal compensating for an increase in $CO_2$. One animal was imaged once with a baseline [11C]PBR28 scan then twice under hypercapnia (7% $CO_2$) conditions. Another animal received one hypercapnia scan and then two baseline scans, with the order of the baseline and hypercapnia sessions reversed in the two animals.

*PET data analysis & kinetic modeling.* All PET images were brought into a standardized NHP space consisting of a population-average MRI-based atlas,[50] based on registration of the MR anatomical image. Template-based ROIs[51] were used to extract time-activity curves (TACs) for the thalamus, prefrontal gray matter, occipital cortex and whole-brain. The thalamus was selected as this region has previously displayed high uptake of [11C]PBR28 in human cLBP patients,[3] the prefrontal cortex was added to ensure inclusion of a cortical binding region, while the whole-brain and occipital cortex have been previously proposed as possible a pseudo-reference regions in the absence of a true reference region for [11C]PBR28.[24]

The effect of hypercapnia on the PET data was assessed in two separate ways: (i) comparing outcome measures (described below) across sessions and animals, and in addition (ii) TACs were evaluated for within-session changes associated with the hypercapnia blocks.

As semi-quantitative outcome measures, standard uptake values (SUV) and tissue ratios (also referred to as SUV ratios (SUVR)) relative to whole-brain or occipital cortex were computed for the scan interval from 65-80 minutes. This interval was chosen to capture the hypercapnia period during this timeframe and to match human studies that typically compute SUVR from ~60–90 minutes.

For full quantification, kinetic modeling was carried out using a 2-tissue compartmental model. First, the plasma input function was metabolite-corrected and fitted using Feng's model.[52] In the two cases with failed arterial blood sampling (see image acquisition section), the plasma input curve from the same animal under the same scanning condition (baseline or hypercapnia scan) was used, after correction for time-delay for each experiment. This method was chosen after inspecting all plasma curves and determining that they were similar within each animal across experiments, except for a time-delay. Region-based kinetic modeling using the extracted TACs was then carried out in PMOD 3.9 (PMOD Technologies LLC, Zurich, Switzerland). The blood volume fraction was

initially fitted to the data and then fixed to $V_b = 0.03$ as this provided a slightly better fit to the data compared to a conventional arbitrary blood volume of 5%. A delay term for the plasma input function was fitted together with kinetic modeling using the 2-tissue compartmental model. Outcome parameters of interest from the 2-tissue compartmental modeling included the plasma-to-tissue rate constant $K_1$, the tissue-to-plasma rate constant $k_2$ and the $V_T$ for each ROI. The latter was used to calculate DVR relative to whole-brain or occipital cortex.

*ASL data analysis.* All pCASL timecourse data were first motion-corrected using AFNI software, spatially smoothed with a 4 mm Gaussian kernel and registered to the same standardized NHP space[50] as the PET images. To compute perfusion-weighted or relative CBF changes, a pairwise subtraction of tag and control data was performed and changes in %CBF were calculated relative to the first 5 min of acquisition. Absolute values of CBF on a voxelwise level were then calculated using the $M_0$ calibration map and the single post-labeling delay according to known methods.[49] Absolute CBF values were extracted as an average for the entire scan duration and for each normocapnia and hypercapnia interval, with a specific focus on the early PET tracer delivery period (1-15 min) and the late interval used for the calculation of PET outcome measures (65–80 min). A combination of MATLAB code (Mathworks, Natick, MA, USA) and open-access software was used for all data analysis and processing.[53]

*Statistical data analysis.* Within the NHP data, correlations between all [11C]PBR28 outcome measures ($K_1$, $k_2$, tissue ratios or SUVR, DVR, SUV, $V_T$) and CBF values were investigated on a regional basis for the thalamus, prefrontal and occipital ROI using a linear regression model. A significance level of $p = 0.05$ was used for all cases. Data normality was assessed using the Shapiro-Wilk test and the quantile-quantile (QQ) plot.

Theory: Relationship between radiotracer delivery parameters and blood flow. Based on existing theoretical frameworks,[34,54,55] the relationship between the plasma-to-tissue rate $K_1$ and blood flow $F$ can be described as:

$$K_1 = E \times F = k_2 \frac{PS_1}{PS_2} \quad (1)$$

Where

$$E = 1 - e^{-\frac{PS}{F}} \quad (2)$$

$$PS_1 = f_p PS_1^0, \text{ (for plasma to tissue), and} \quad (3)$$

$$PS_2 = f_{ND} PS_2^0, \text{ (for tissue to plasma)} \quad (4)$$

If $PS_1^0 \approx PS_2^0$, it follows that

$$K_1 = f_p K_1^0 \quad (5)$$

where E is the extraction of the radiotracer, F is blood flow, PS is the permeability-surface area product, $f_p$ is the plasma free fraction, $f_{ND}$ is the free fraction in the non-displaceable tissue compartment and $K_1^0$ is the true rate with all tracer freely available for transport in plasma (i.e. $f_p = 1$). As stated in equation (1), the plasma-to-tissue rate $K_1$ is linearly dependent on both blood flow and extraction. The latter is non-linearly dependent on blood flow and may be further affected by blood flow through changes in permeability and surface area with flow. Moreover, the value of $K_1$ depends on the free fraction of radiotracer in plasma (equation (5)). If either E or $f_p$ is low, the effect of blood flow on $K_1$ is inherently limited by that fraction.

## Results

### Human subjects

A voxel-wise comparison of CBF values from pCASL maps between cLBP patients vs. healthy controls using stringent statistical thresholding (cluster-forming threshold: $z = 3.1$; cluster size threshold: $p = 0.05$) did not reveal any significant group differences in perfusion (whether using absolute or whole-brain normalized CBF maps). Even when relaxing the cluster-forming threshold to $z = 2.3$, voxelwise group comparisons of absolute CBF maps revealed no group differences. However, using this lenient threshold, analyses of whole-brain normalized CBF maps did reveal areas of hypoperfusion (but no hyperperfusion) in cLBP patients compared to healthy controls, in a cluster encompassing motor cortex, supplementary motor area, anterior and posterior cingulate cortices, and corticospinal tracts (Figure 1 and Table 1). Notably, even at the more lenient threshold, no significant group differences in CBF signal were apparent in the thalamus, the region exhibiting the most consistent [11C]PBR28 signal elevations in our previous cLBP studies using the outcome measures SUVR[3] or $V_T$.[24] Whole-brain normalized CBF values in the hypoperfusion cluster were $0.82 \pm 0.19$ (mean $\pm$ SD) for the cLBP patients and $1.06 \pm 0.14$ for the healthy controls. Despite the lower CBF values, [11C]PBR28 SUVR (60-90 min, with whole-brain as the "pseudoreference") was not significantly different between groups in this hypoperfusion
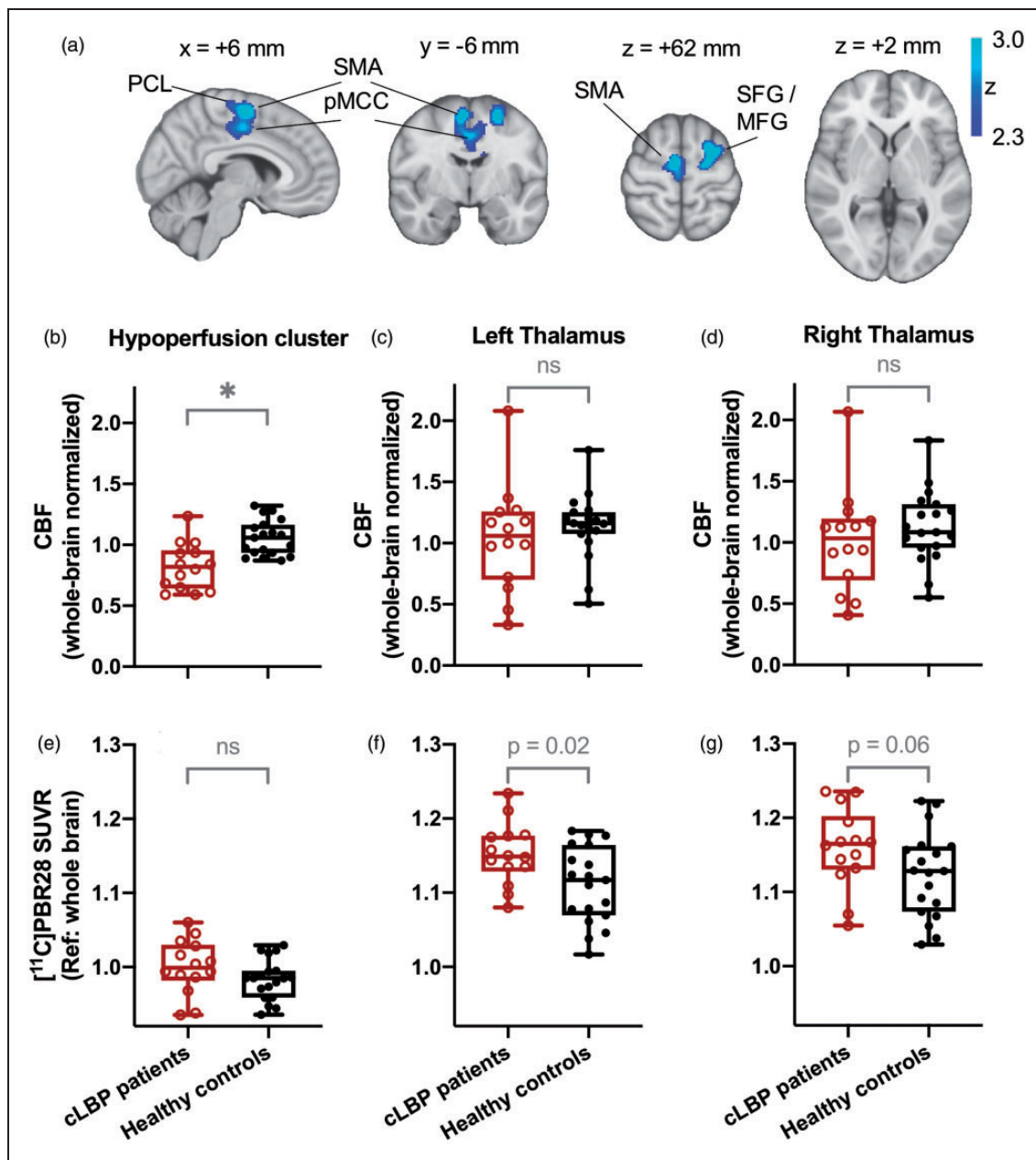
**Figure 1.** (a) Areas characterized by hypoperfusion in chronic low back pain (cLBP) patients compared to healthy controls (HC). The significant hypoperfusion cluster comprises the supplementary motor area, posterior cingulate gyrus, middle frontal gyrus and superior frontal gyrus. Group comparisons of CBF measurements between CLBP patients and healthy controls show an increase in CBF in the hypoperfusion cluster (b) but not in the thalamus (c,d). (e,f,g) Elevated [$^{11}$C]PBR28 SUV ratios (SUVR, relative to whole brain) were found in cLBP patients in the hypoperfusion cluster and the left thalamus but were not accompanied by increases in CBF. *Notations:* ✳: significant in voxelwise analyses (cluster-forming threshold of $z = 2.3$ and cluster size threshold of $p = 0.05$); ns: not significant; SFG: superior frontal gyrus; MFG: middle frontal gyrus; SMA: supplementary motor area; PCL: paracentral lobule.

cluster ($p = 0.18$), with a mean SUVR of $1.00 \pm 0.04$ in the cLBP patients vs. $0.98 \pm 0.03$ in the healthy controls. Similarly, no significant differences were found between groups for SUVR with occipital cortex as a reference, with a mean SUVR of $0.94 \pm 0.06$ in the cLBP patients vs. $0.92 \pm 0.06$ in the healthy controls.

While a thalamus-focused ROI analysis did not yield any group differences using whole-brain normalized nor absolute CBF values (Figure 1(c) and (d)), in the same subjects we confirmed the presence of elevated thalamic [$^{11}$C]PBR28 SUVR (with whole-brain as the reference) in cLBP compared to controls.

**Table 1.** CBF reductions in cLBP patients (hypoperfusion cluster).

| # Voxels | $p$ value | $z_{max}$ value | x (mm) | y (mm) | z (mm) | Label |
|---|---|---|---|---|---|---|
| 2364 | 0.0104 | 3.5 | −26 | 0 | 62 | L SFG / MFG |
| | | 3.48 | 6 | −6 | 60 | R SMA |
| | | 3.13 | 12 | −12 | 46 | R pMCC |
| | | 2.78 | 2 | −20 | 64 | R PCL |
| | | 2.71 | 2 | 10 | 36 | R aMCC |

SFG: superior frontal gyrus; MFG: middle frontal gyrus; SMA: supplementary motor area; pMCC: posterior middle cingulate cortex; PCL: paracentral lobule; aMCC: anterior middle cingulate cortex.
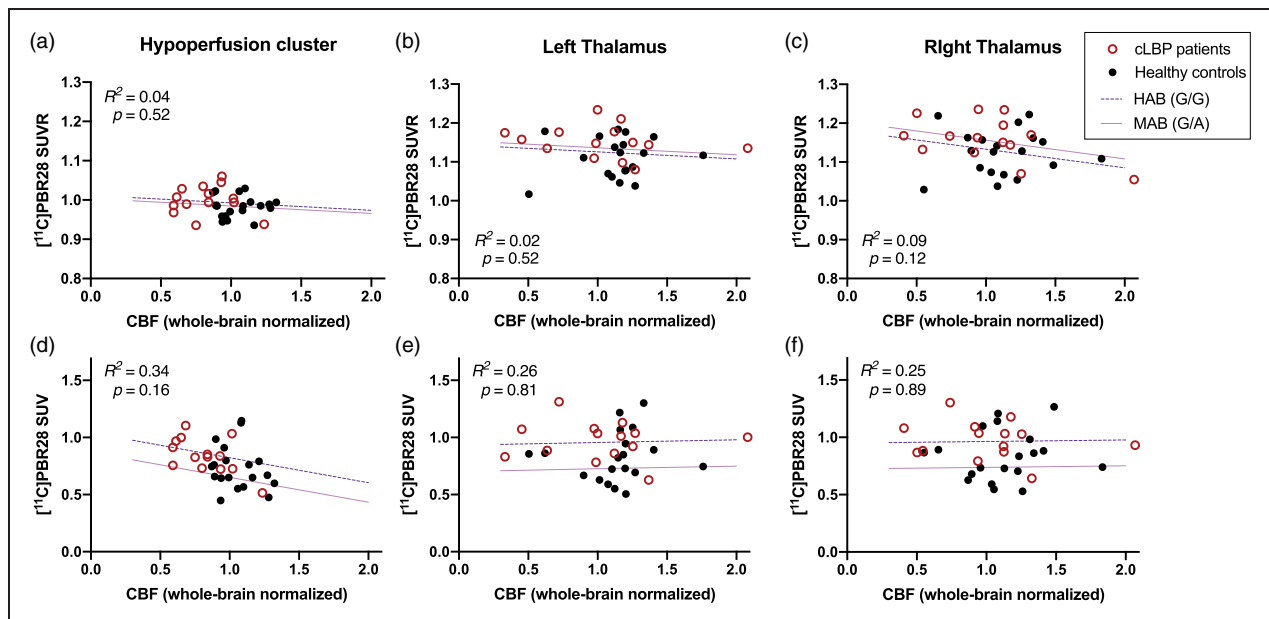


**Figure 2.** Scatterplot of [$^{11}$C]PBR28 tissue ratios (relative to whole brain, 60–90 min post-injection) vs. cerebral blood flow (CBF) acquired from pseudo-continuous arterial spin labelling for the hypoperfusion cluster (a), left thalamus (b) and right thalamus (c). Equivalent scatterplots of standard uptake values (SUVs) vs. CBF are shown for the same regions (d–f). No significant correlations between [$^{11}$C]PBR28 tissue ratios or SUV and blood flow were detected, after adjusting for genotype, suggesting that TSPO signal elevations are not accompanied by increases in CBF in CLBP patients or controls. HAB: high affinity binders, MAB: medium affinity binders.

These differences were statistically significant in the left thalamus ($p = 0.02$ with mean SUVR of $1.15 \pm 0.04$ in the cLBP patients and $1.11 \pm 0.05$ in the healthy controls) and trended towards significance in the right thalamus ($p = 0.06$ with mean SUVR of $1.16 \pm 0.05$ in the cLBP patients and $1.12 \pm 0.06$ in the healthy controls; see Figure 1(f) and (g)). Significance levels in this study were set to $p = 0.05$. Using the occipital cortex as a reference for the SUVR calculation, similar results were observed with a significantly higher SUVR in the left thalamus ($p = 0.045$ with mean SUVR of $1.09 \pm 0.08$ in the cLBP patients and $1.05 \pm 0.09$ in the healthy controls) and a marginally higher SUVR in the right thalamus ($p = 0.07$ with mean SUVR of $1.10 \pm 0.09$ in the cLBP patients and $1.06 \pm 0.09$ in the healthy controls).

Correlation analyses between SUVR and normalized CBF were not significant, including genotype as a covariate, neither for the hypoperfusion cluster ($R^2 = 0.04$, $p = 0.52$) nor for the left thalamus ($R^2 = 0.02$, $p = 0.52$) or right thalamus ROI ($R^2 = 0.09$, $p = 0.12$) (Figure 2(a) to (c)). Equivalent analyses using SUV and normalized CBF did not yield significant correlations either (Figure 2(d) to (f)). Even though cLBP patients and healthy controls showed a relatively wide distribution of absolute CBF values that spanned from approximately 10–50 mL/100g/min, corresponding SUVRs or SUVs did not exhibit a linear relationship with CBF.

## Non-human primates

Among the hypercapnia experiments, but not during baseline scans, we observed significant increases in CBF during hypercapnia intervals, indicating that the experimental manipulation with 7% $CO_2$ was successful. Absolute whole-brain CBF values were on average $92 \pm 14$ mL/100g/min during normocapnia and $121 \pm 15$ mL/100g/min during hypercapnia intervals. Figure 3 shows representative experimental data from one baboon for a baseline (blue) and a hypercapnia session (red) for the thalamus and the whole-brain. Experimental data from all six experimental sessions in the two animals are shown in Supplemental Material (Figure S1). The %CBF changes during the hypercapnia intervals are clearly visible through elevated %CBF (Figure 3(a) and (b)) during administration of 7% $CO_2$. Despite large changes in %CBF up to 100% increase, the corresponding [$^{11}$C]PBR28 TACs from baseline and hypercapnia sessions are very similar (Figure 3(c) and (d)), indicating two findings: (i) [$^{11}$C]PBR28 pharmacokinetics across visits do not show measurable differences between the hypercapnia vs. baseline scan and (ii) the CBF change pattern reflecting the normo- vs. hypercapnia blocks within an experimental session are not observed in the [$^{11}$C]PBR28 TAC dynamics. For the two scans in Figure 3, [$^{11}$C]PBR28 tissue ratios from 65–80 min for thalamus/whole-brain are 1.16 at baseline and 1.10 during the hypercapnia scan. Absolute CBF values during this interval were 73 mL/100g/min (thalamus), 104 mL/100g/min (whole-brain) at baseline and 97 mL/100g/min (thalamus), 112 mL/100g/min (whole-brain) for the hypercapnia scan.

We evaluated the radiotracer delivery parameters during different blood flow conditions through quantification using a 2-tissue compartmental model. As a main finding, neither the plasma-to-tissue rate constant
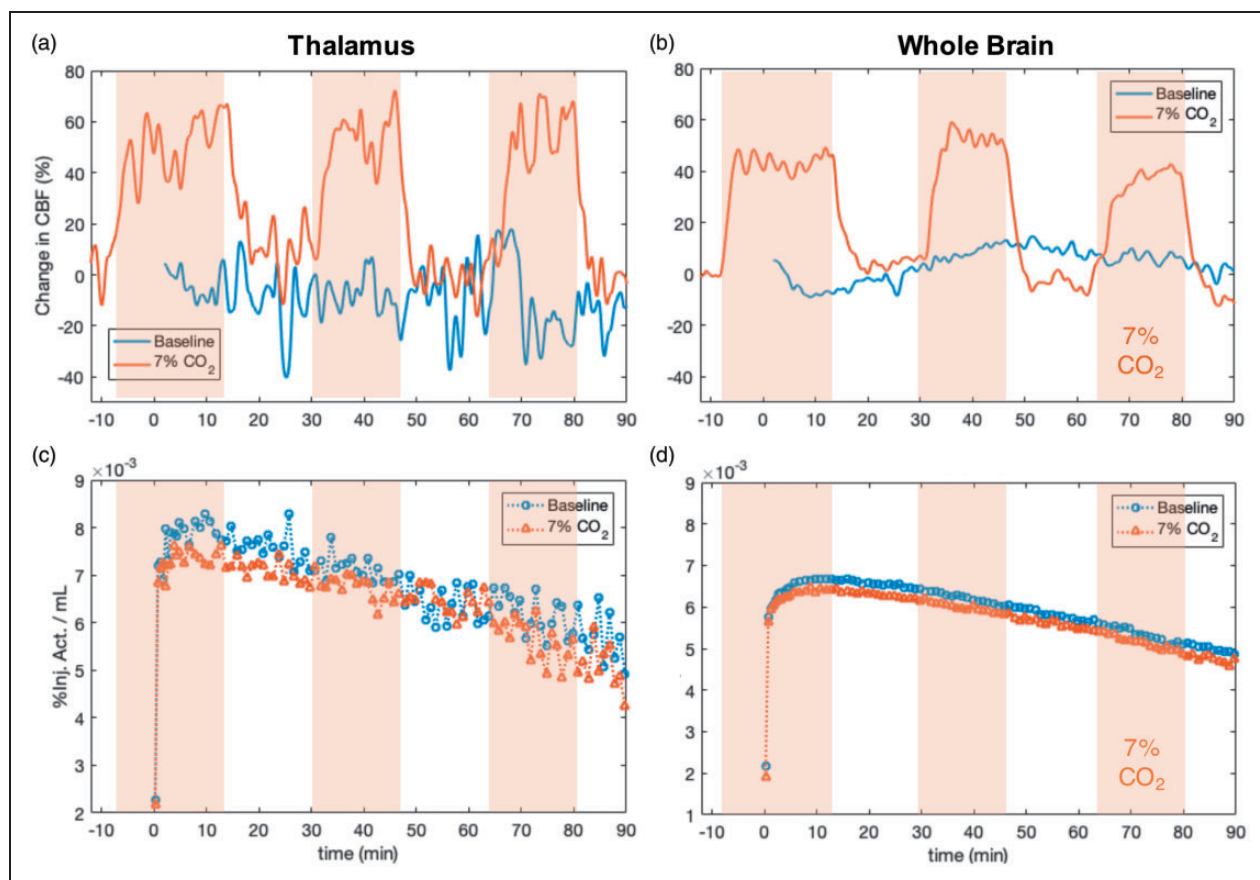


**Figure 3.** (a, b): Relative cerebral blood flow changes (CBF) as measured with pCASL (smoothed with a Gaussian kernel across 16 points) from two experimental sessions that include baseline and hypercapnia conditions from one representative animal. Hypercapnia periods (delineated as orange shaded areas) clearly show increased CBF (orange line) compared to a baseline scan without hypercapnia (blue line), both in the thalamus and across whole brain. (c, d): Corresponding, simultaneously acquired, time activity curves (TACs) from two bolus injections of [$^{11}$C]PBR28, shown for the thalamus and the whole brain. The baseline TACs (blue circles) and the TACs with hypercapnia intervention (orange triangles) are similar in magnitude and shape, with no detectable changes observed despite the increased CBF.

$K_1$ nor the tissue-to-plasma rate constant $k_2$ showed values that were elevated with higher blood flow. Figure 4(a) and (b) shows the rate constants from each experimental session for direct comparison purposes in each animal. Average values of $K_1$ and $k_2$ are listed in Table 2 for the thalamus, prefrontal gray matter (GM) and occipital cortex. For the whole brain, $K_1$ values were $0.11 \pm 0.02$ vs. $0.11 \pm 0.00$ ml/cm$^3$/min in the baseline vs. hypercapnia sessions, respectively. Average values of $k_2$ for the baseline vs. hypercapnia sessions were $0.06 \pm 0.02$ vs. $0.08 \pm 0.02$ min$^{-1}$ in whole-brain, respectively. To assess relevant blood flow parameters, we modulated and measured CBF during the radiotracer delivery and uptake period. During the first 15 minutes after TOI, CBF was increased during all hypercapnia sessions compared to baseline scans (Figure 4(d)). Absolute CBF values (mean $\pm$ SD) during these first 15 min for the baseline vs. hypercapnia sessions were $92 \pm 2$ vs. $118 \pm 19$ ml/100g/min in the whole-brain (thalamus, prefrontal GM and occipital ROI values are listed in Table 2).

For all three hypercapnia blocks (0–15 min, 30–45 min, 65–80 min) in the hypercapnia sessions, CBF was increased compared to the equivalent times in the baseline sessions. Figure 4(e) shows the comparison for the 65–90 min hypercapnia block. The average CBF measurement for the entire scan time of 90 minutes is shown in Figure 4(f). In these comparisons, mean CBF from the entire duration of the scan is reported, which includes both hypercapnia and normocapnia intervals, and thus show smaller fluctuations on average compared to hypercapnia-only intervals.

A linear regression between $K_1$ or $k_2$ and CBF values did not reveal correlations between these parameters in any of the ROIs. Figure 4(c) visualizes the relation between $K_1$ and the CBF data from the first 15 minutes for the four ROIs, together with the regression line for just the thalamus ROI, which has a coefficient of determination of $R^2 = 0.09$. The correlation between $k_2$ and the first 1–15 min CBF measurement resulted in an $R^2 = 0.16$ (Figure S2 in Supplemental Material).
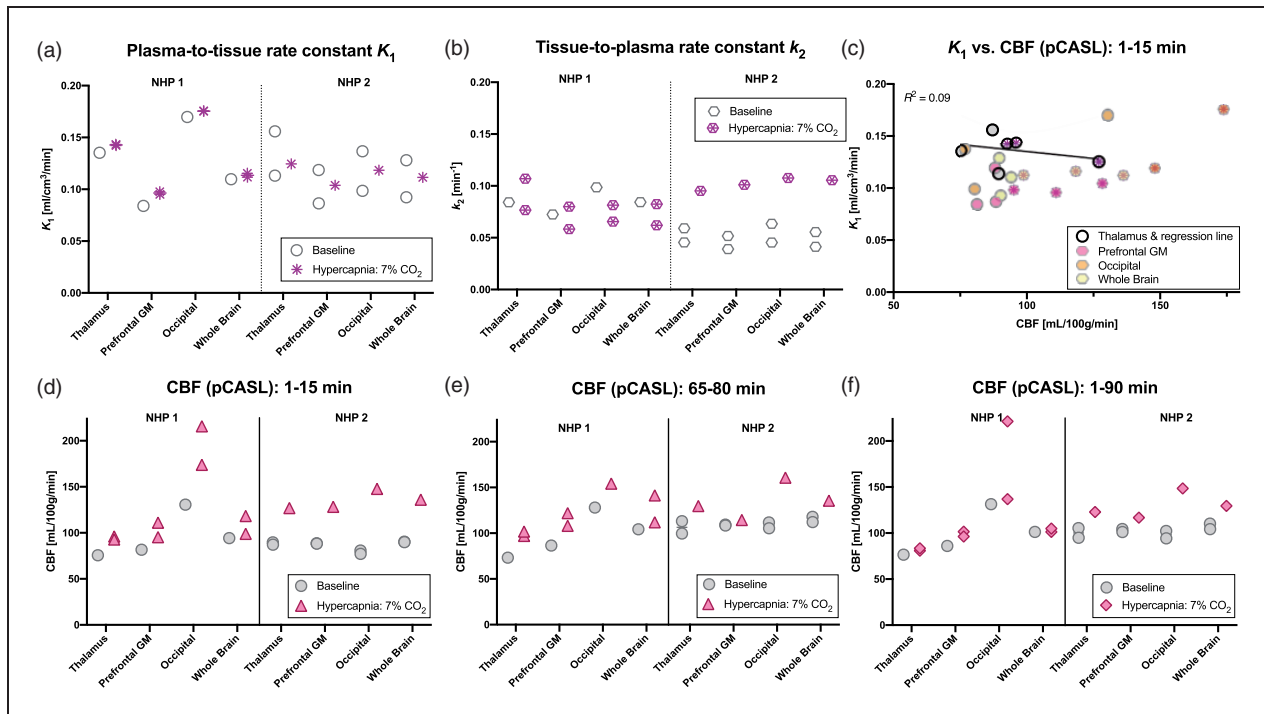


**Figure 4.** [$^{11}$C]PBR28 delivery and washout rate constants (derived form a 2-tissue compartmental model), and simultaneously acquired cerebral blood flow (CBF) values (measured with pseudo-continuous arterial spin labeling (pCASL)) in two non-human primates (NHP), in a total of six imaging sessions. (a) Estimates of the plasma-to-tissue delivery rate constant $K_1$ do no show increases in $K_1$ at baseline versus hypercapnia conditions. (b) Estimates of the tissue-to-plasma rate constant $k_2$ show larger variation, with a small decrease in NHP 1 and an increase in NHP 2, but no consistent pattern with higher blood flow values. (c) Comparisons between $K_1$ and CBF from the first 1–15 min do not display evident correlations for any of the regions. The regression line for the thalamus is displayed for visualization. (d, e) CBF values show consistently increased blood flow during the hypercapnia periods applied at the beginning (1–15 min) of the hypercapnia scan during tracer delivery and during the late 65–80 min interval compared to baseline scans. (f) Average CBF values for the entire duration of the scan are only slightly increased due to the hypercapnia periods being interleaved with baseline normal air levels.

**Table 2.** [$^{11}$C]PBR28 kinetic parameters and outcome measures for baseline vs. hypercapnia sessions together with cerebral blood flow (CBF) measurements in the non-human primates.

| | Thalamus | | Prefrontal gray matter | | Occipital cortex | |
|---|---|---|---|---|---|---|
| | Baseline | Hypercapnia | Baseline | Hypercapnia | Baseline | Hypercapnia |
| $K_1$ (ml/cm$^3$/min) | 0.13 ± 0.02 | 0.14 ± 0.01 | 0.1 ± 0.02 | 0.1 ± 0.00 | 0.14 ± 0.04 | 0.16 ± 0.03 |
| $k_2$ (min$^{-1}$) | 0.06 ± 0.02 | 0.09 ± 0.02 | 0.05 ± 0.02 | 0.08 ± 0.02 | 0.07 ± 0.03 | 0.08 ± 0.02 |
| $V_T$ | 8.5 ± 2.6 | 6.7 ± 1.9 | 7.4 ± 3.1 | 5.7 ± 1.5 | 7.4 ± 1.3 | 7.1 ± 2.6 |
| DVR | | | | | | |
| (Ref: whole-brain) | 1.1 ± 0.0 | 1.1 ± 0.1 | 1.0 ± 0.1 | 0.9 ± 0.1 | 1.0 ± 0.2 | 1.1 ± 0.1 |
| (Ref: occipital) | 1.1 ± 0.2 | 1.0 ± 0.2 | 1.0 ± 0.3 | 0.8 ± 0.2 | n/a | n/a |
| SUV$^{[65-90\,min]}$ | 1.3 ± 0.2 | 1.1 ± 0.1 | 1.0 ± 0.2 | 0.9 ± 0.2 | 1.2 ± 0.1 | 1.2 ± 0.2 |
| SUVR$^{[65-90\,min]}$ (Ref: whole-brain) | 1.2 ± 0.0 | 1.1 ± 0.0 | 0.9 ± 0.1 | 0.9 ± 0.1 | 1.1 ± 0.2 | 1.2 ± 0.2 |
| SUVR$^{[65-90\,min]}$ (Ref: occipital) | 1.1 ± 0.2 | 0.9 ± 0.1 | 0.9 ± 0.2 | 0.8 ± 0.2 | n/a | n/a |
| CBF$^{[1-15\,min]}$ (ml/100g/min) | 84 ± 8 | 105 ± 19 | 86 ± 4 | 112 ± 16 | 96 ± 30 | 179 ± 34 |
| CBF$^{[65-80\,min]}$ (ml/100g/min) | 95 ± 20 | 109 ± 18 | 101 ± 13 | 115 ± 7 | 115 ± 12 | 201 ± 76 |

Note: Average values (with standard deviation) for the plasma-to-tissue rate constant $K_1$, the tissue-to-plasma rate constant $k_2$, volume of distribution ($V_T$), distribution volume ratios (DVR), standard uptake value (SUV for 65–90 min) and corresponding tissue ratios (SUVR), with whole-brain and occipital cortex as a reference (ref), are shown for three regions of interest. Absolute cerebral blood flow (CBF) values obtained with pseudo-continuous arterial spin labeling are shown for the first 15 min and for the 65–80 min periods. Data from a total of 6 experimental sessions obtained in two animals are shown, with baseline and hypercapnia values representing n = 3 sessions each (see Methods for further details).

Given the experimentally determined delivery and blood flow parameters in the non-human primate experiments, we determined extraction of [$^{11}$C]PBR28 to be $E_{PBR28} = 0.14$. This was calculated using the relationship described in equation (1) and average baseline parameter values from the thalamus ROI from our experiments: $K_1 = 0.13$ ml/cm$^3$/min and CBF = 0.9 ml/g/min.

The two main outcome measures we evaluated were tissue ratios (SUVR) and distribution volume ratios (DVR) as outcome parameters that are commonly used in clinical [$^{11}$C]PBR28 studies. In both cases, ratios of ROIs were computed relative to the whole-brain or occipital cortex following previously published methods due to the lack of a true reference region devoid of TSPO for [$^{11}$C]PBR28. Both SUVRs and DVR were found to be robust measurements and repeated measurements found very similar values for both outcome measures (Figure 5(a) and (b)). Average tissue ratios (SUVR) and DVRs for the thalamus, prefrontal and occipital cortex relative to whole-brain for the baseline vs. hypercapnia sessions are shown in Table 2. As an alternative outcome, the same outcome parameters for the thalamus and prefrontal cortex are also shown relative to the occipital cortex.

Correlations between SUVR and CBF, both from the 65–80 min scan interval, did not reveal an obvious linear relationship for any of the ROIs ($R^2 = 0.37$ for the thalamus, Figure 5(c)). Similarly, DVR and CBF from the early 1–15 min interval did not exhibit correlations for any of the ROIs ($R^2 = 0.04$ for the thalamus, Figure 5(d)). For the latter comparison, we used CBF measurements from the early timepoint since these showed the largest increases, thus representing the most extreme scenario. Correlations with CBF measurements from other timepoints did not show correlations either.

Considering the effect of blood flow on alternative outcome measures, we compared CBF data to absolute SUV and $V_T$, which is shown in Figure S3 in Supplemental Material. As expected, both SUV and $V_T$ values showed more variability compared to the outcome measures based on ratios. Despite the variability in these outcome measures, we did not observe any consistent relationship to increases in CBF. Linear regressions for each ROI did not yield any significant correlations, neither for SUV vs. CBF for the 65-80 min interval, nor for $V_T$ vs. CBF for the first 1-15 min interval (Figure S3). Mean SUV values for 65-80 min were on average 1.3 ± 0.2 (thalamus), 1.0 ± 0.2 (prefrontal), 1.2 ± 0.1 (occipital), 1.1 ± 0.2 (whole-brain) during baseline sessions and 1.1 ± 0.1 (thalamus), 0.9 ± 0.2 (prefrontal), 1.2 ± 0.2 (occipital), 1.0 ± 0.1 (whole-brain) during hypercapnia sessions. Mean $V_T$ values were 8.5 ± 2.6 (thalamus), 7.4 ± 3.1 (prefrontal), 7.4 ± 1.3 (occipital), 7.5 ± 2.5 (whole-brain) during baseline sessions and 6.7 ± 1.9 (thalamus), 5.7 ± 1.5 (prefrontal), 7.1 ± 2.6 (occipital), 6.2 ± 1.7 (whole-brain) during hypercapnia sessions.
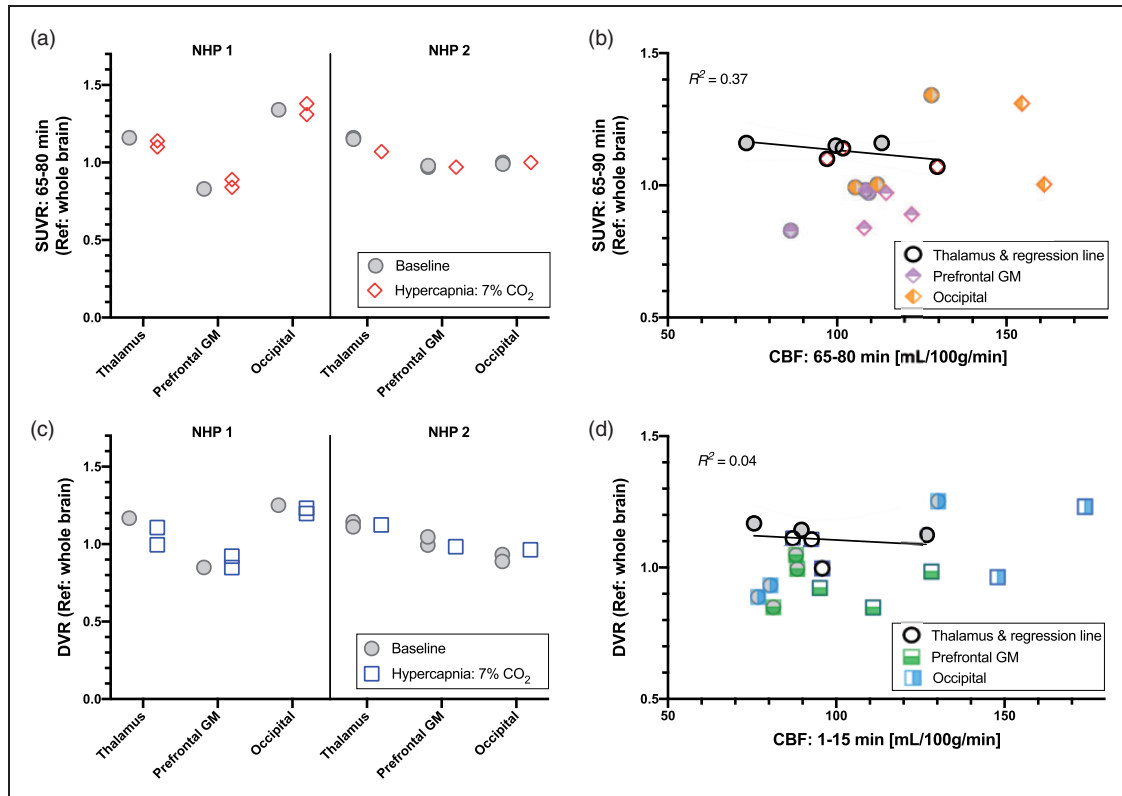
**Figure 5.** (a) Tissue ratios (SUVR) relative to whole brain from the 65–80 min scan interval show almost identical values between baseline and hypercapnia conditions for each region of interest (thalamus, prefrontal gray matter (GM) and occipital cortex) in each animal. (b) Linear regressions between SUVR and cerebral blood flow (CBF) from the 65–80 scan interval do not show obvious correlations in any of the three regions (regression line shown for thalamus ROI). (c) The distribution volume ratio (DVR) shows robust outcome measurements that have similar values between baseline and hypercapnia experimental sessions. This suggests that neither outcome measurement is noticeably influenced by changes in cerebral blood flow. (d) DVR was not correlated to CBF from the 1–15 min scan interval in any of the regions, suggesting no dependency of these outcome measures on CBF.

## Discussion

In this study, we investigated associations between and effects of CBF changes on [11C]PBR28 delivery parameters, radiotracer kinetics and outcome measures. In humans, our results did not reveal any statistically significant correlations between [11C]PBR28 signal and CBF, even in marginally hypoperfused areas in the brain of cLBP patients. These results support the absence of a meaningful influence of CBF on the [11C]PBR28 signal, suggesting that the [11C] PBR28 elevation observed in CLBP patients are reflective of a genuine regional upregulation of the glial marker TSPO. In non-human primates, we deliberately increased CBF using a 7% $CO_2$ hypercapnia challenge to investigate any causal relationships between CBF changes and [11C]PBR28 parameters. Despite large increases in CBF, we did not observe consistent differences in time activity curves, radiotracer delivery parameters or outcome parameters between baseline sessions and sessions with increased CBF. Based on visual inspection, no correlations were found between

[11C]PBR28 micro- or macro-parameters or semi-quantitative outcome measures with CBF measurements; we note that sample sizes in the NHP dataset are not sufficiently large for statistical inference. Still, this dataset provides insight as it spans a large range in CBF values due to the hypercapnia intervention, with little variation in PET parameters. Overall, the results from this study suggest that changes in CBF do not affect [11C]PBR28 signal, and support our contention that [11C]PBR28 outcome parameters are not driven by blood flow effects, and reflect genuine differences in TSPO binding.

Using combined PET/MR imaging allowed for concurrent measurements of CBF and [11C]PBR28 signals in cLBP patients and healthy controls, and we were able to directly compare CBF values to [11C]PBR28 SUV and SUVR outcome measures in the same individuals during the same scan. While elevations in [11C] PBR28 signals as well as changes in CBF in cLBP patients have been reported from separate studies, this is the first time a concurrent measurement of

CBF and [11C]PBR28 signals is reported and directly compared to our knowledge. In our cohort of cLBP patients, we did not find significant elevations in CBF in any brain regions (including in the thalamus, i.e., the region exhibiting the most consistent TSPO signal elevations in cLBP[3]). Rather, we solely observed reduced CBF in a localized cluster, and only when using a liberal threshold. The lack of robust CBF differences in cLBP patients and controls at baseline (i.e., in the absence of a pain challenge) is compatible with previous results from our group, in which statistically significant increases in CBF were reported only after the performance of clinical maneuvers that exacerbated the patients back pain, but not prior to the challenge.[20] While the evaluation of patients at baseline meant that we could not directly evaluate the effect of CBF increases in cLBP patients, we did evaluate the association between TSPO signal and CBF measurements in correlational analyses. Overall, the fact that CBF values were not correlated with [11C]PBR28 SUV or SUVR measures provides support for [11C]PBR28 signal elevations (observed in this and previously published studies[3,11]) not being driven by CBF, and truly representing TSPO upregulation.

Importantly, the statistics employed on the human data in our study were designed to reject the null hypothesis, not to conclude equivalence (i.e., that two groups do not differ). For this reason, a larger, well-powered study allowing for the implementation of equivalence tests will be required to conclude that, for instance, resting thalamic perfusion in cLBP patients is equivalent to that of pain-free healthy controls. Still, our current study does allow us to conclude that we are unable to detect statistically significant group differences in CBF between groups, despite the presence of statistically significant differences in [11C]PBR28 signal, suggesting that the former does not have a sizable impact on the latter.

As a complementary arm of this study, our non-human primate experiments were designed to test a causal link between elevated CBF and [11C]PBR28 pharmacokinetics and outcome parameters. Hypercapnia interventions are a well-established methodology for inducing large and robust increases in CBF.[56,57] For physiological stability and safety of the animals, it was most feasible to administer 7% $CO_2$ in blocks rather than continuously for the entire duration of the experiment. Hence, we focused on increasing CBF during crucial time periods of 15 minutes each, which were during radiotracer uptake at the beginning of the PET scan and at later timepoints when clinical semi-quantitative outcome measurements are usually recorded. The large CBF changes within each scan allowed us to exclude within-scan effects of CBF fluctuations on [11C]PBR28, whereas comparisons between separate baseline and hypercapnia sessions suggested no dependency of pharmacokinetic rate constants or outcome measures on CBF. While hypercapnia-induced CBF increases may not be driven by the exact same mechanism as CBF changes caused by disease or variations in normal physiology, we expect that the effect of such large CBF increases as we observed to have similar effect on radiotracer delivery and washout and be representative of other induced CBF changes that could occur.

Limitations of this study include the use of anesthesia and small sample size in the non-human primate experiments. Both of these factors are driven by practical challenges in carrying out the animal studies. While anesthesia represents a separate state from the awake brain and may influence absolute levels of [11C]PBR28 uptake,[58] our main question of investigation – the response to large changes in CBF – were evaluated both within and across animals under the same anesthetic conditions and are thus expected to provide valid insights for translational results. While our overall sample size was small, driven by ethical constraints in the use of NHPs, the effect size of the increases in CBF is very large and can be observed at the single session level. Results were derived from repeated scanning of animals in addition to comparisons from within-session hypercapnia blocks, providing insightful results that are not just driven by the number of independent imaging sessions. Moreover, in two cases, we employed a time-delay-corrected plasma input curve (under same baseline or hypercapnia conditions) from the same animal but a separate session, where arterial blood sampling was not acquired for the full duration of the experiment. This may have contributed to additional variability of the reported results but, inspection of the data indicated that it did not impact conclusions that would have been drawn if these experiments had been excluded from the study.

The results from this study are concordant with theoretical predictions: Given that the plasma-to-tissue rate constant $K_1$ and thus extraction fraction of [11C]PBR28 (as calculated from experimentally determined $K_1$ and CBF in this study) are relatively low ($K_1 = 0.13$, $E = 0.14$) compared to flow tracers, even large changes in blood flow are expected to only have a small, and thus probably not measurable, effect on $K_1$. We also note that our reported $K_1$ values are in the same range as previously reported values in the literature.[55,59] Moreover, since the plasma free fraction $f_p$ of [11C]PBR28 has been reported to be small, around 3-5%[60] for humans and non-human primates, and $K_1$ is limited by this parameter (see equation (5)), we again expect blood flow to have a minimal impact. In line with these predictions, in this study, we provided experimental measurements of $K_1$ and $k_2$ together with concurrently

acquired CBF measurements and showed that these microparameters did not show a measurable dependency on CBF even over a large range of blood flow values. Theoretically predicted small changes in $K_1$ due to blood flow further have a negligible effect on macroparameters when it is assumed that $K_1$ and $k_2$ are both proportionally affected by changes in blood flow, as has been shown in simulations for other radiotracers.[37,61,62] Finally, for other TSPO radiotracers that are characterized by similarly small $K_1$ and/or $f_p$ values as [11C]PBR28, we would also expect a lack of blood flow dependence on delivery and outcome parameters: For example, [11C]ER176 has been reported to have a similar $K_1$,[59] while [11C]-(R)-PK11195, [18F]GE180 (both have a very low $f_p$ of 1-3%), as well as [11C]DAA1106 are known to have a $K_1$ that is at least ten-fold lower.[55,63] Given these characteristics, we would expect the delivery of these radiotracers to not be driven by alterations in CBF, similar to [11C]PBR28. Even though the TSPO ligand [11C]DPA-713 has a reported $K_1$ on the order of 0.25, with an $f_p$ of 9%,[55] this is still likely not sufficiently large to show flow sensitivity for physiologically relevant flow changes, given the large range of blood flow values we have studied here and previously.[37]

Overall, the lack of a statistically significant correlation between radiotracer outcome measures and blood flow is in line with results reported in the literature. Our group previously demonstrated that the dopaminergic radiotracers [11C]raclopride and [18F]fallypride do not show a dependency on CBF, as measured with pCASL.[37] Similarly, delivery parameters and blood flow were not found to be significantly correlated in a study comparing $K_1$ values from [11C]PiB and [15O]water.[64] While the latter and other studies found positive correlations between relative CBF measurements from [15O]water and the relative delivery parameter $R_1$[65,65] or early frame amyloid radiotracer data,[66,67] these results are consistent with normalized delivery parameters being a surrogate for normalized CBF. The latter is not equivalent to a direct dependency of $K_1$ on blood flow. Overall, our results that $K_1$ and radiotracer outcome parameters are not significantly associated with physiological changes in CBF as determined by pCASL is in agreement with existing study findings both in terms of experimental results as well as from a theoretical perspective.

## Conclusion

In summary, our study evaluated associations between CBF and [11C]PBR28 signal in humans, contrasting cLBP patients vs. healthy controls. Through simultaneous acquisitions of CBF and [11C]PBR28, we found that [11C]PBR28 signal changes are not correlated with CBF. Secondly, in non-human primates, we deliberately increased CBF using a hypercapnia challenge without finding changes in [11C]PBR28 pharmacokinetic microparameters or outcome measures. Together, these results provide evidence that neither [11C]PBR28 pharmacokinetics nor (semi-) quantitative outcome measures are affected by fluctuations in CBF, thereby supporting the interpretation of elevated [11C]PBR28 signals as genuine upregulation of the glial marker TSPO.

## Declaration of conflicting interests

The author(s) declared no potential conflicts of interest with respect to the research, authorship, and/or publication of this article.

## Authors' contributions

CYS and MLL designed the study. CYS, SB, ATC, DA, HPD and MLL acquired experimental data and analyzed the imaging data. CYS, SB, ATC, DA, VN, JCP and JMH contributed to interpreting the data. CYS drafted the article together with MLL and all authors revised it critically for important intellectual content.

## Supplementary material

Supplemental material for this article is available online.

## ORCID iDs

Christin Y Sander https://orcid.org/0000-0001-6003-8615
Stefano Bovo https://orcid.org/0000-0002-0278-6786
Angel Torrado-Carvajal https://orcid.org/0000-0002-1540-2809
Helen P Deng https://orcid.org/0000-0002-9752-8965

## References

1. Brown AK, Fujita M, Fujimura Y, et al. Radiation dosimetry and biodistribution in monkey and man of

11C-PBR28: a PET radioligand to image inflammation. *J Nucl Med* 2007; 48: 2072–2079.

2. Briard E, Zoghbi SS, Imaizumi M, et al. Synthesis and evaluation in monkey of two sensitive 11C-labeled aryloxyanilide ligands for imaging brain peripheral benzodiazepine receptors in vivo. *J Med Chem* 2008; 51: 17–30.

3. Loggia ML, Chonde DB, Akeju O, et al. Evidence for brain glial activation in chronic pain patients. *Brain* 2015; 138: 604–615.

4. Albrecht DS, Ahmed SU, Kettner NW, et al. Neuroinflammation of the spinal cord and nerve roots in chronic radicular pain patients. *Pain* 2018; 159: 968–977.

5. Zürcher NR, Loggia ML, Lawson R, et al. Increased in vivo glial activation in patients with amyotrophic lateral sclerosis: assessed with [11C]-PBR28. *Neuroimage Clin* 2015; 7: 409–414.

6. Albrecht DS, Granziera C, Hooker JM, et al. In vivo imaging of human neuroinflammation. *ACS Chem Neurosci* 2016; 7: 470–483.

7. Kreisl WC, Lyoo CH, McGwier M, et al. In vivo radioligand binding to translocator protein correlates with severity of Alzheimer's disease. *Brain* 2013; 136: 2228–2238.

8. Varrone A, Oikonen V, Forsberg A, et al. Positron emission tomography imaging of the 18-kDa translocator protein (TSPO) with [18F]FEMPA in Alzheimer's disease patients and control subjects. *Eur J Nucl Med Mol Imaging* 2015; 42: 438–446.

9. Lois C, González I, Izquierdo-García D, et al. Neuroinflammation in Huntington's disease: new insights with 11C-PBR28 PET/MRI. *ACS Chem Neurosci* 2018; 9: 2563–2571.

10. Albrecht DS, Forsberg A, Sandström A, et al. Brain glial activation in fibromyalgia – a multi-site positron emission tomography investigation. *Brain Behav Immun* 2019; 75: 72–83.

11. Albrecht DS, Kim M, Akeju O, et al. The neuroinflammatory component of negative affect in patients with chronic pain. *Mol Psychiatry* 2021; 26: 864–874.

12. Albrecht DS, Mainero C, Ichijo E, et al. Imaging of neuroinflammation in migraine with aura: a [11 C]PBR28 PET/MRI study. *Neurology* 2019; 92: e2038–e2050.

13. Narendran R, Lopresti BJ, Mason NS, et al. Cocaine abuse in humans is not associated with increased microglial activation: an 18-kDa translocator protein positron emission tomography imaging study with [11C]PBR28. *J Neurosci* 2014; 34: 9945–9950.

14. Hillmer AT, Sandiego CM, Hannestad J, et al. In vivo imaging of translocator protein, a marker of activated microglia, in alcohol dependence. *Mol Psychiatry* 2017; 22: 1759–1766.

15. Kalk NJ, Guo Q, Owen D, et al. Decreased hippocampal translocator protein (18kDa) expression in alcohol dependence: a [11C]PBR28 PET study. *Transl Psychiatry* 2017; 7: e996–e996.

16. Bloomfield PS, Selvaraj S, Veronese M, et al. Microglial activity in people at ultra high risk of psychosis and in schizophrenia: an [11C]PBR28 PET brain imaging study. *Am J Psychiatry* 2016; 173: 44–52.

17. Collste K, Plavén-Sigray P, Fatouros-Bergman H, Karolinska Schizophrenia Project (KaSP) consortium, et al. Lower levels of the glial cell marker TSPO in drug-naive first-episode psychosis patients as measured using PET and [11C]PBR28. *Mol Psychiatry* 2017; 22: 850–856.

18. Notter T, Coughlin JM, Gschwind T, et al. Translational evaluation of translocator protein as a marker of neuroinflammation in schizophrenia. *Mol Psychiatry* 2018; 23: 323–334.

19. Plavén-Sigray P, Matheson GJ, Collste K, et al. Positron emission tomography studies of the glial cell marker translocator protein in patients with psychosis: a meta-analysis using individual participant data. *Biol Psychiatry* 2018; 84: 433–442.

20. Wasan AD, Loggia ML, Chen LQ, et al. Neural correlates of chronic low back pain measured by arterial spin labeling. *Anesthesiology* 2011; 115: 364–374.

21. Michels L, Villanueva J, O'Gorman R, et al. Interictal hyperperfusion in the higher visual cortex in patients with episodic migraine. *Headache* 2019; 59: 1808–1820.

22. Rizzo G, Veronese M, Tonietto M, et al. Kinetic modeling without accounting for the vascular component impairs the quantification of [11C]PBR28 brain PET data. *J Cereb Blood Flow Metab* 2014; 34: 1060–1069.

23. Veronese M, Reis Marques T, Bloomfield PS, et al. Kinetic modelling of [11C]PBR28 for 18 kDa translocator protein PET data: a validation study of vascular modelling in the brain using XBD173 and tissue analysis. *J Cereb Blood Flow Metab* 2018; 38: 1227–1242.

24. Albrecht DS, Normandin MD, Shcherbinin S, et al. Pseudoreference regions for glial imaging with 11C-PBR28: investigation in 2 clinical cohorts. *J Nucl Med* 2018; 59: 107–114.

25. Alshelh Z, Albrecht DS, Bergan C, et al. In-vivo imaging of neuroinflammation in veterans with Gulf war illness. *Brain Behav Immun* 2020; 87: 498–507.

26. Woodcock EA, Schain M, Cosgrove KP, et al. Quantification of [11C]PBR28 data after systemic lipopolysaccharide challenge. *EJNMMI Res* 2020; 10: 1–6.

27. Matheson GJ, Plavén-Sigray P, Forsberg A, et al. Assessment of simplified ratio-based approaches for quantification of PET [11C]PBR28 data. *EJNMMI Res* 2017; 7: 6.

28. Yoder KK, Territo PR, Hutchins GD, et al. Comparison of standardized uptake values with volume of distribution for quantitation of [11C]PBR28 brain uptake. *Nucl Med Biol* 2015; 42: 305–308.

29. Tóth M, Doorduin J, Häggkvist J, et al. Positron emission tomography studies with [11C]PBR28 in the healthy rodent brain: validating SUV as an outcome measure of neuroinflammation. *PLoS One* 2015; 10: e0125917–14.

30. Schain M, Zanderigo F, Ogden RT, et al. Non-invasive estimation of [11C]PBR28 binding potential. *Neuroimage* 2018; 169: 278–285.

31. Plavén-Sigray P, Schain M, Zanderigo F, et al. Accuracy and reliability of [11 C]PBR28 specific binding estimated without the use of a reference region. *Neuroimage* 2019; 188: 102–110.

32. Lyoo CH, Ikawa M, Liow JS, et al. Cerebellum can serve as a pseudo-reference region in Alzheimer disease to detect neuroinflammation measured with PET radioligand binding to translocator protein. *J Nucl Med* 2015; 56: 701–706.

33. Cumming P, Xiong G, Fougère CL, et al. Surrogate markers for cerebral blood flow correlate with [18F]-fallypride binding potential at dopamine D2/3 receptors in human striatum. *Synapse* 2013; 67: 199–203.

34. Logan J, Volkow ND, Fowler JS, et al. Effects of blood flow on [11C]raclopride binding in the brain: model simulations and kinetic analysis of PET data. *J Cereb Blood Flow Metab* 1994; 14: 995–1010.

35. Koeppe RA, Frey KA, Snyder SE, et al. Kinetic modeling of N-[11C]methylpiperidin-4-yl propionate: alternatives for analysis of an irreversible positron emission tomography trace for measurement of acetylcholinesterase activity in human brain. *J Cereb Blood Flow Metab* 1999; 19: 1150–1163.

36. Fowler JS, Logan J, Wang GJ, et al. Comparison of the binding of the irreversible monoamine oxidase tracers, [11C]clorgyline and [11C]l-deprenyl in brain and peripheral organs in humans. *Nucl Med Biol* 2004; 31: 313–319.

37. Sander CY, Mandeville JB, Wey HY, et al. Effects of flow changes on radiotracer binding: simultaneous measurement of neuroreceptor binding and cerebral blood flow modulation. *J Cereb Blood Flow Metab* 2019; 39: 131–146.

38. Owen DR, Yeo AJ, Gunn RN, et al. An 18-kDa translocator protein (TSPO) polymorphism explains differences in binding affinity of the PET radioligand PBR28. *J Cereb Blood Flow Metab* 2012; 32: 1–5.

39. Izquierdo-Garcia D, Hansen AE, Förster S, et al. An SPM8-based approach for attenuation correction combining segmentation and nonrigid template formation: application to simultaneous PET/MR brain imaging. *J Nucl Med* 2014; 55: 1825–1830.

40. Buxton RB, Frank LR, Wong EC, et al. A general kinetic model for quantitative perfusion imaging with arterial spin labeling. *Magn Reson Med* 1998; 40: 383–396.

41. Chappell MA, Groves AR, Whitcher B, et al. Variational bayesian inference for a nonlinear forward model. *IEEE Trans Signal Process* 2009; 57: 223–236.

42. Andersson JLR, Jenkinson M and Smith S. Non-linear registration aka spatial normalisation. *FMRIB Tech Rep TR07JA2* 2007; 22: 1–21.

43. Ssali T, Anazodo UC, Bureau Y, et al. Mapping long-term functional changes in cerebral blood flow by arterial spin labeling. *PLoS One* 2016; 11: e0164112–18.

44. Michels L, Warnock G, Buck A, et al. Arterial spin labeling imaging reveals widespread and A$\beta$-independent reductions in cerebral blood flow in elderly apolipoprotein epsilon-4 carriers. *J Cereb Blood Flow Metab* 2016; 36: 581–595.

45. Chen Y, Wolk DA, Reddin JS, et al. Voxel-level comparison of arterial spin-labeled perfusion MRI and FDG-PET in Alzheimer disease. *Neurology* 2011; 77: 1977–1985.

46. Patenaude B, Smith SM, Kennedy DN, et al. A Bayesian model of shape and appearance for subcortical brain segmentation. *Neuroimage* 2011; 56: 907–922.

47. Woolrich MW, Behrens TEJ, Beckmann CF, et al. Multilevel linear modelling for FMRI group analysis using Bayesian inference. *Neuroimage* 2004; 21: 1732–1747.

48. Sander CY, Keil B, Chonde DB, et al. A 31-channel MR brain array coil compatible with positron emission tomography. *Magn Reson Med* 2015; 73: 2363–2375.

49. Wey H-Y, Wang DJ and Duong TQ. Baseline CBF, and BOLD, CBF, and CMRO2 fMRI of visual and vibrotactile stimulations in baboons. *J Cereb Blood Flow Metab* 2011; 31: 715–724.

50. McLaren DG, Kosmatka KJ, Oakes TR, et al. A population-average MRI-based atlas collection of the rhesus macaque. *Neuroimage* 2009; 45: 52–59.

51. Sullivan EV, Grant KA, Bowden DM, et al. The INIA19 template and NeuroMaps atlas for primate brain image parcellation and spatial normalization. *Front Neuroinform* 2012; 6: 1–15.

52. Feng D, Huang SC and Wang X. Models for computer simulation studies of input functions for tracer kinetic modeling with positron emission tomography. *Int J Biomed Comput* 1993; 32: 95–110.

53. JIP fMRI Analysis Toolkit, http://www.nitrc.org/projects/jip (accessed 25 May 2021).

54. Mintun MA, Raichle ME, Kilbourn MR, et al. A quantitative model for the in vivo assessment of drug binding sites with positron emission tomography. *Ann Neurol* 1984; 15: 217–227.

55. Endres CJ, Pomper MG, James M, et al. Initial evaluation of 11C-DPA-713, a novel TSPO PET ligand, in humans. *J Nucl Med* 2009; 50: 1276–1282.

56. Tancredi FB, Lajoie I and Hoge RD. Test-retest reliability of cerebral blood flow and blood oxygenation level-dependent responses to hypercapnia and hyperoxia using dual-echo pseudo-continuous arterial spin labeling and step changes in the fractional composition of inspired gases. *J Magn Reson Imaging* 2015; 42: 1144–1157.

57. Ito H, Kanno I, Ibaraki M, et al. Changes in human cerebral blood flow and cerebral blood volume during hypercapnia and hypocapnia measured by positron emission tomography. *J Cereb Blood Flow Metab* 2003; 23: 665–670.

58. Hines CS, Fujita M, Zoghbi SS, et al. Propofol decreases in vivo binding of 11C-PBR28 to translocator protein (18 kDa) in the human brain. *J Nucl Med* 2013; 54: 64–69.

59. Zanotti-Fregonara P, Pascual B, Veronese M, et al. Head-to-head comparison of 11C-PBR28 and 11C-ER176 for quantification of the translocator protein in the human brain. *Eur J Nucl Med Mol Imaging* 2019; 46: 1822–1829.

60. Fujita M, Imaizumi M, Zoghbi SS, et al. Kinetic analysis in healthy humans of a novel positron emission tomography radioligand to image the peripheral benzodiazepine receptor, a potential biomarker for inflammation. *Neuroimage* 2008; 40: 43–52.

61. Normandin MD, Schiffer WK and Morris ED. ED. A linear model for estimation of neurotransmitter response profiles from dynamic PET data. *Neuroimage* 2012; 59: 2689–2699.

62. Alpert NM, Badgaiyan RD, Livni E, et al. A novel method for noninvasive detection of neuromodulatory changes in specific neurotransmitter systems. *Neuroimage* 2003; 19: 1049–1060.

63. Zanotti-Fregonara P, Pascual B, Rizzo G, et al. Head-to-head comparison of 11C-PBR28 and 18F-GE180 for quantification of the translocator protein in the human brain. *J Nucl Med* 2018; 59: 1260–1266.

64. Chen YJ, Rosario BL, Mowrey W, et al. Relative 11C-PiB delivery as a proxy of relative CBF: quantitative evaluation using single-session 15o-water and 11C-PiB PET. *J Nucl Med* 2015; 56: 1199–1205.

65. Bilgel M, Beason-Held L, An Y, et al. Longitudinal evaluation of surrogates of regional cerebral blood flow computed from dynamic amyloid PET imaging. *J Cereb Blood Flow Metab* 2020; 40: 288–297.

66. Rodriguez-Vieitez E, Carter SF, Chiotis K, et al. Comparison of early-phase 11C-Deuterium-L-Deprenyl and 11C-Pittsburgh compound B PET for assessing brain perfusion in alzheimer disease. *J Nucl Med* 2016; 57: 1071–1077.

67. Forsberg A, Engler H, Blomquist G, et al. The use of PIB-PET as a dual pathological and functional biomarker in AD. *Biochim Biophys Acta* 2012; 1822: 380–385.